PAPER

Ternary selenides $A_2Sb_4Se_8$ (A = K, Rb and Cs) as an n-type thermoelectric material with high power factor and low lattice thermal conductivity: importance of the conformationally flexible Sb–Se–Se–Sb bridges†

Changhoon Lee, [iD] ‡[a] Sujee Kim,‡[b] Won-Joon Son, [iD][c] Ji-Hoon Shim*[a] and Myung-Hwan Whangbo*[def]

We investigated the thermoelectric properties of the layered ternary selenides $A_2Sb_4Se_8$ (A = K, Rb and Cs) and the lattice thermal conductivity of $K_2Sb_4Se_8$ on the basis of DFT calculations, to find that these selenides are a high-performance n-type thermoelectric material. The Seebeck coefficients and power factors calculated for the electron carriers of $A_2Sb_4Se_8$ (A = K, Rb and Cs) are greater than those of the well-known thermoelectric materials Bi_2Te_3 and PbTe. The lattice thermal conductivity κ_{latt} of $K_2Sb_4Se_8$ is comparable to that of PbTe, well-known for its low lattice thermal conductivity. In terms of both electronic and phonon structures, the structural parts of the $A_2Sb_4Se_8$ (A = K, Rb and Cs) phases crucial for their thermoelectric properties are the conformationally-flexible Sb–Se–Se–Sb bridges that interlink between their structurally rigid units.

Introduction

Thermoelectricity enables a direct conversion between thermal and electrical energies, so materials exhibiting thermoelectricity have received much attention for power generation and cooling.[1,2] In particular, thermoelectric power generation is potentially important for waste heat collection and efficient energy utilization, although its application is limited due to the low efficiency of thermoelectric devices. The efficiency of a thermoelectric material at a given temperature T depends on the figure of merit, $ZT = S^2\sigma T/\kappa$, where σ, κ and S are the electrical conductivity, the thermal conductivity and the Seebeck coefficient, respectively.[3] The amount of power generated by a thermoelectric material is related to the power factor, $S^2\sigma$, which is the major element governing the magnitude of ZT.[4]

Another element raising the ZT is a low thermal conductivity κ, which is composed of the electric thermal conductivity (κ_{el}) and the lattice thermal conductivity (κ_{latt}), that is, $\kappa = \kappa_{el} + \kappa_{latt}$. κ_{el} is directly proportional to the carrier concentration, n, because $\kappa_{el} \propto \sigma$ via the Wiedemann–Franz law, $\kappa_{el} = L\sigma T$,[5] where L is Lorenz number, and because $\sigma \propto n$. In general, a high figure of merit ZT requires a compromise between the carrier concentration and the thermal conductivity.[6,7] In terms of the carrier densities affecting the thermoelectric properties of a material, the electronic states lying close to its conduction band minimum (CBM) and valence band maximum (VBM) (*i.e.*, those typically within ~0.5 eV of the CBM or the VBM) are found to be crucial.[8] From the viewpoint of understanding the structure–property relationship governing the thermoelectric properties of a material,

---

[a]Department of Chemistry, Pohang University of Science and Technology, Pohang, 37673, Korea. E-mail: jhshim@postech.ac.kr

[b]Division of Advanced Nuclear Engineering, Pohang University of Science and Technology, Pohang, 37673, Korea

[c]Samsung Advanced Institute of Technology (SAIT), Samsung Electronics, 130 Samsung-ro, Yeongtong-gu, Suwon 16678, Korea

[d]Department of Chemistry, North Carolina State University, Raleigh, NC, 27695-8204, USA. E-mail: whangbo@ncsu.edu

[e]State Key Laboratory of Structural Chemistry, Fujian Institute of Research on the Structure of Matter (FJIRSM), Chinese Academy of Sciences (CAS), Fuzhou, 350002, China

[f]State Key Laboratory of Crystal Materials, Shandong University, Jinan, 250100, China

it is important to find which structural part of the material is largely responsible for those states close to the CBM and VBM.

The binary tellurides Bi_2Te_3 (ref. 9a) and PbTe[9b] are well-known efficient thermoelectric materials. It is of interest and importance to search for a potential high-performance thermoelectric material that can be as efficient as Bi_2Te_3 and PbTe. In the present work we carry out DFT calculations to explore the thermoelectric properties of the layered ternary selenide $K_2Sb_4Se_8$ (ref. 10) as well as its isostructural phases $Rb_2Sb_4Se_8$ (ref. 11a) and $Cs_2Sb_4Se_8$.[11b] As depicted in Fig. 1, $K_2Sb_4Se_8$ consists of Sb_4Se_8 layers separated by K^+, and each layer is made up of $Sb(1)Se_4$ seesaw units, $Sb(2)Se_3$ pyramids, and Se_2 dimers. There are two types of cross-linked rings in each Sb_4Se_8 layer; one is the 12-membered ring made up of two $Sb(1)_2Se_6$ and two $Sb(2)Se_3$ units, and the other is the 14-membered ring made up of four $Sb(2)Se_3$, two $Se(2)_2$ and two $Sb(1)Se_4$ seesaw units. From the viewpoint of understanding the lattice thermal conductivity of $K_2Sb_4Se_8$, it is more convenient to consider each Sb_4Se_8 layer in terms of the "Sb_4Se_6" chains made up of cross-linked 12-membered rings, which run along the b-direction. For clarity, one Sb_4Se_6 repeat unit of this chain is colored in grey in Fig. 1. When these Sb_4Se_6 chains are bridged by the $Se(2)_2$ dimers to form 14-membered rings between the Sb_4Se_6 chains, we obtain the Sb_4Se_8 layer.

Since the Sb–$Se(2)$–$Se(2)$–Sb bridges have a high conformational flexibility (namely, a soft potential energy curve with respect to a small variation in the dihedral angle $\angle Sb$–$Se(2)$–$Se(2)$–Sb), it is expected that the Sb_4Se_8 layer is more rigid along the Sb_4Se_6 chain direction (i.e., along the b-direction for

$K_2Sb_4Se_8$) than along the interchain direction [i.e., along the $(a + c)$-direction for $K_2Sb_4Se_8$]. In addition, the $K_2Sb_4Se_8$ crystal should be least rigid along the interlayer direction because there is no covalent bonding between adjacent Sb_4Se_8 layers. In this low-dimensional structure of $K_2Sb_4Se_8$ as determined by X-ray diffraction, the unit cell parameters are large so that the lattice thermal conductivity would be low with short mean path for acoustic phonons.[12] Thus, it is worthwhile investigate the possibility that $K_2Sb_4Se_8$ as well as its two isostructural selenides, $Rb_2Sb_4Se_8$ and $Cs_2Sb_4Se_8$, are a high-performance thermoelectric material. In the present work, we examine the Seebeck coefficients and power factors of $A_2Sb_4Se_8$ (A = K, Rb, Cs) and the lattice thermal conductivity of $K_2Sb_4Se_8$ on the basis of DFT calculations, to predict that the ternary selenides $A_2Sb_4Se_8$ (A = K, Rb, Cs) are a high-performance thermoelectric material comparable in efficiency to, or better than, the well-known thermoelectric materials Bi_2Te_3 and PbTe.

Details of calculations

Our DFT calculations employed the frozen-core projector augmented wave (PAW) method[13] encoded in the Vienna ab initio simulation package (VASP),[14] with the generalized-gradient approximation (GGA)[15] of Perdew, Burke and Ernzerhof (PBE) for the exchange–correlation functional and the plane-wave-cut-off energy of 450 eV. The BoltzTrap code[16] was used to calculate the thermoelectric properties of all $K_2Sb_4Se_8$ systems, which solves the semi-classical Boltzmann equation using the rigid band approach.[17,18] This method has been successful in calculating the transport properties and predicting the optimal doping levels for thermoelectric materials.[17–20] To ensure the convergence of the calculated thermoelectric properties, the irreducible Brillouin zone was sampled by a set of 2000 k-points. The BoltzTrap code allows one to calculate the electrical conductivity σ, the Seebeck coefficient S, and the power factor $S^2\sigma/\tau$ under the assumption that the electron momentum relaxation time τ is independent of energy. We employ the latter assumption, because there is currently no information about the τ of $A_2Sb_4Se_8$. The power factors calculated under this assumption are greater than the experimental values,[21] but this overestimation arises in part from the fact that the band gaps are under estimated by DFT calculations. We note that the thermoelectric properties of numerous systems have been explained by using this assumption.[22] We simulate the phonon behavior of $K_2Sb_4Se_8$ by using the frozen phonon method implemented in Phono3py[23] to investigate the lattice thermal conductivity.

Electronic structures

The electronic structure calculated for $K_2Sb_4Se_8$ is presented in terms of the total density of states (DOS) in Fig. 2a, and in terms of band dispersion relations in Fig. 2b along several wave vector directions of the first Brillouin zone (Fig. 2c). $K_2Sb_4Se_8$ has a band gap of ~1.0 eV. The projected DOS (PDOS) calculated for the Sb and Se atoms of $K_2Sb_4Se_8$ are presented in Fig. 3. The PDOS plots for the Se(1), Se(3) and Se(4) are very similar but

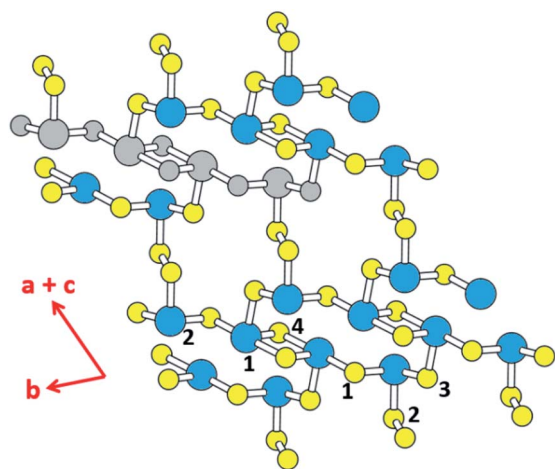**Fig. 1** Schematic diagram showing the structure of the Sb_4Se_8 layer of $K_2Sb_4Se_8$. The large and small circles represent the Sb and Se atoms, respectively. The Sb(1) and Sb(2) atoms are represented by blue circles, and Se(1)−Se(4) atoms by yellow circles, except for one Sb_4Se_6 unit. The latter is indicated by grey circles for both Sb and Se, for clarity. The Sb_4Se_8 layer is composed of 12- and 14-membered rings that are cross-linked. The cross-linked 12-membered rings form the Sb_4Se_6 chains running along the b-direction. The Sb_4Se_6 chains are linked by Se_2 dimers to form 14-membered rings that are cross-linked. It should be noted that the b- and $(a + c)$-crystallographic directions of $K_2Sb_4Se_8$ are the same as those of $Rb_2Sb_4Se_8$, but correspond to the a- and $(b−c)$-directions of $Cs_2Sb_4Se_8$, respectively.
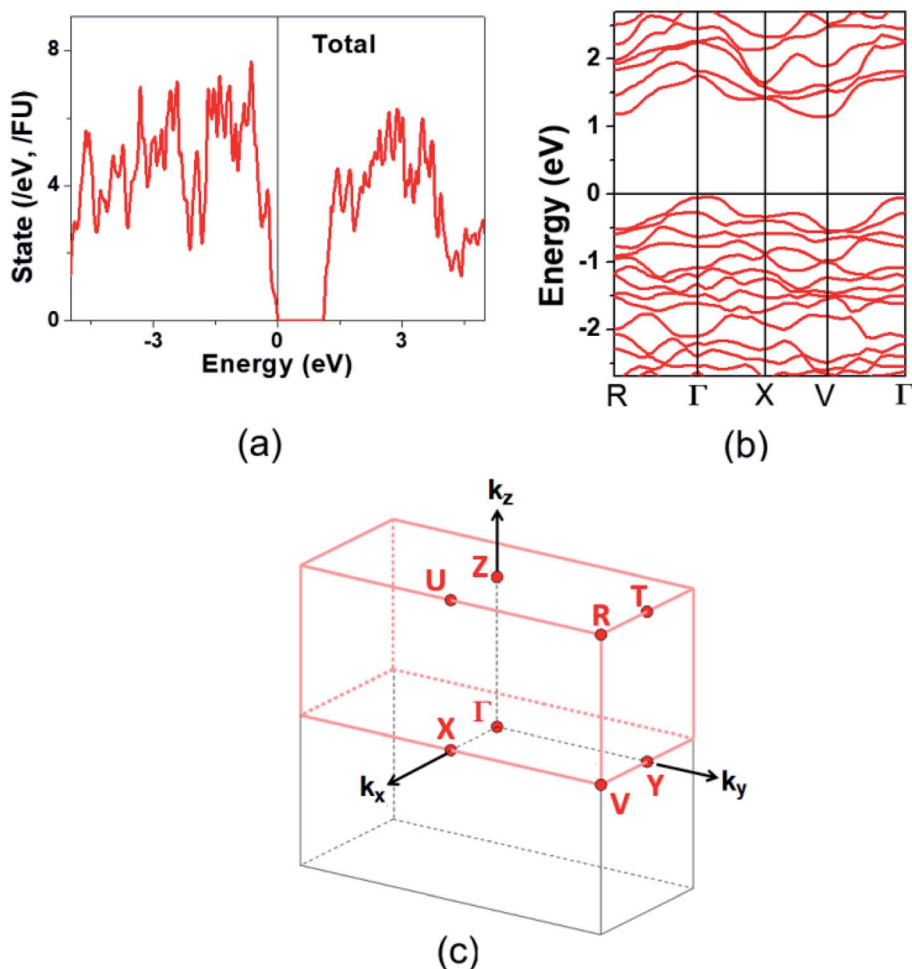
Fig. 2 Electronic structure calculated for $K_2Sb_4Se_8$: (a) Total DOS plot. (b) Band dispersion relations. (c) First Brillouin zone associated with a crystal lattice of space group $P\bar{1}$.

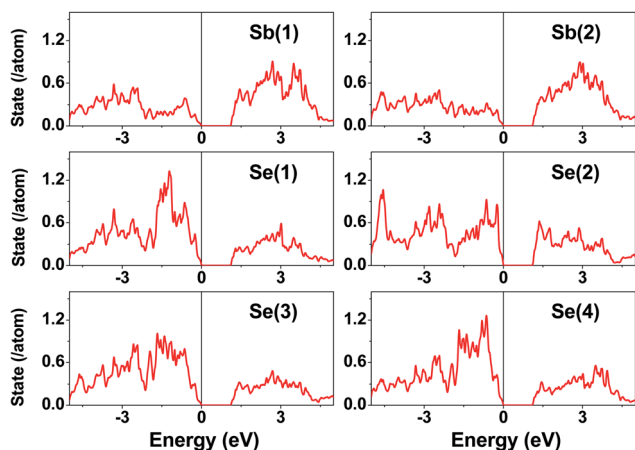**Fig. 3** PDOS plots calculated for the Sb(1), Sb(2), Se(1), Se(2), Se(3), and Se(4) atoms of $K_2Sb_4Se_8$.

differ considerably from that for Se(2). In the occupied states of the PDOS, the Se(1), Se(3), and Se(4) each show two band blocks, which represent the bonding states between Sb and Se and the

nonbonding states of Se. In contrast, the Se(2) shows roughly three band blocks, which arise from the Se(2)–Se(2) bonding states in addition to the Se–Sb bonding and the Se nonbonding states.

This reflects that the formal oxidation state of Se(1), Se(3), and Se(4) atoms is −2 whereas that of the Se(2) is −1. At the CBM and VBM, the Se(2) contributes more strongly than does the Se(1), Se(3) or Se(4) atom, and than does the Sb(1) or Sb(2) atom. Since the thermoelectric properties of a material are mainly influenced by the electronic states lying very close to its CBM and VBM (*i.e.*, typically those within ~0.5 eV from the VBM and CBM),[8] the thermoelectric properties of $K_2Sb_4Se_8$ should be strongly influenced by the electronic structures associated with the $Se(2)_2$ dimer units. The total DOS plots of $Rb_2Sb_4Se_8$ and $Cs_2Sb_4Se_8$, presented in Fig. S1 in the ESI,† are very similar to that of $K_2Sb_4Se_8$ presented in Fig. 2.

Thermoelectric properties

We calculate the Seebeck coefficients of $A_2Sb_4Se_8$ (A = K, Rb, Cs) at 300 K as a function of the chemical potential μ. In terms of the rigid band approximation, the electron density can be

introduced into $A_2Sb_4Se_8$ by raising the Fermi level E_f from the CBM, so the chemical potential μ defined as $\mu = E_f - CBM$, with the electron density $n(\mu)$ given by

$$n(\mu) = \frac{1}{V} \int_0^\mu N(E)dE$$

where V is the unit cell volume, and $N(E)$ the total DOS at energy E. Similarly, the hole density can be introduced into $A_2Sb_4Se_8$ by lowering the Fermi level E_f from the VBM, so the chemical potential μ is defined as $\mu = VBM - E_f$, with the hole density $p(\mu)$ given by

$$p(\mu) = \frac{1}{V} \int_\mu^0 N(E)dE$$

The μ-dependence of the Seebeck coefficients S calculated for $K_2Sb_4Se_8$ (Fig. 4a) shows two peaks at $\mu \approx \pm 0.061$ eV with $S \approx \pm 1700$ μV K^{-1}. These values are considerably greater than those of the well-known thermoelectric materials Bi_2Te_3 (the calculated $S \approx \pm 250$ μV K^{-1})[16] and PbTe (the calculated $S \approx \pm 350$ μV K^{-1}).[20] The dependence of S on the electron density and that on the hole density (Fig. 4b) reveals that the S decreases in magnitude steadily with increasing either the electron or the hole density. Under the assumption that the relaxation times τ is energy-independent, we calculate the power factor $S^2\sigma/\tau$. The calculated $S^2\sigma/\tau$ is presented as a function of μ (Fig. 4c) and as a function of the carrier density (Fig. 4d). The power factor for the electron carriers is

considerably greater than that for the hole carriers (e.g., the n-type $S^2\sigma/\tau$ is larger than the p-type $S^2\sigma/\tau$ by a factor of ~2). This reflects that the electrical conductivity for the electron carriers is much greater than that for the hole carriers. The Seebeck coefficients and the power factors calculated for $Rb_2Sb_4Se_8$ and $Cs_2Sb_4Se_8$ are summarized in Fig. S2, S3, and S5 in the ESI,† respectively. They are very similar to those described for $K_2Sb_4Se_8$ described above.

We also investigated the temperature dependence of the Seebeck coefficients S and the power factor $S^2\sigma/\tau$ for $A_2Sb_4Se_8$ for A = K, Rb and Cs (Fig. S5 in the ESI†). In comparing these values of the three compounds, it is necessary to consider the possible uncertainties in their carrier densities. Thus, we calculate the Seebeck coefficients S and the power factor $S^2\sigma/\tau$ for different carrier densities within the range between 1×10^{19} to 5×10^{20} cm^{-3}. Fig. S5† reveals that, for both electron and hole carriers, the Seebeck coefficients S and the power factor $S^2\sigma/\tau$ (in the upper and down panels, respectively) gradually increases with temperature. This is due to the increase in thermal energy. The power factor for the electron carriers is considerably greater than that for the hole carriers reflecting that the electrical conductivity for the electron carriers is much greater than that for the hole carriers.

The band dispersion relations calculated for $K_2Sb_4Se_8$ (Fig. 2b) show that $K_2Sb_4Se_8$ has an indirect band gap with the CBM at the M point and the VBM at the Γ point. The VBM has a hole valley at Γ, while the CBM has an electron valley and pseudo electron valley at M and R, respectively. The presence of flat band dispersion relations enhances the DOS and hence the
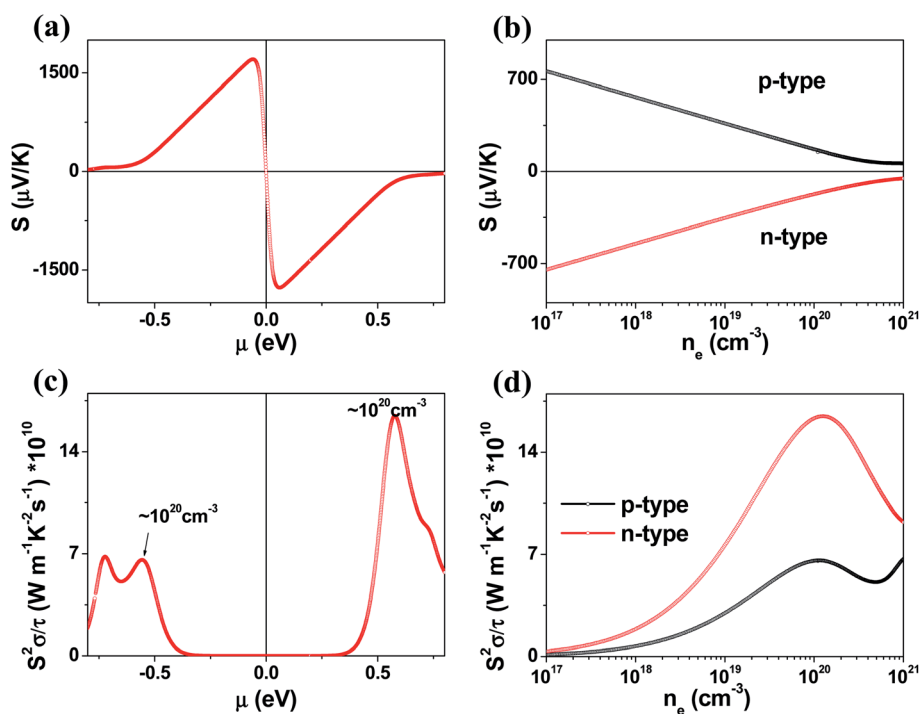

Fig. 4 Thermodynamic properties of $K_2Sb_4Se_8$ calculated at 300 K: (a) Seebeck coefficient S as function of the chemical potential μ. (b) Seebeck coefficient S as function of the carrier density n. (c) Power factor $S^2\sigma/\tau$ as function of the chemical potential μ. (d) Power factor $S^2\sigma/\tau$ as function of the carrier density n.

carrier density. Since the CBM has more valleys than does the VBM, the carrier concentration should be enhanced near the CBM,[24] so that the electrical conductivity is higher for the electrons than for the holes. This explains why the n-type power factor is considerably higher than the p-type power factor despite that the calculated Seebeck coefficients for the hole and electron carriers are similar. The band dispersion relations of $Rb_2Sb_4Se_8$ and $Cs_2Sb_4Se_8$, presented in Fig. S4 in the ESI,† are very similar to that of $K_2Sb_4Se_8$ described above.

Lattice thermal conductivity

In general, a low lattice thermal conductivity κ_{latt} is found for a low dimensional material with heavy elements and large unit cell parameters. $K_2Sb_4Se_8$ is such a material. As already discussed (see Fig. 1), each Sb_4Se_8 layer of $K_2Sb_4Se_8$ is more rigid along the Sb_4Se_6 chain direction (i.e., the b-direction for $K_2Sb_4Se_8$) than along the interchain direction within a Sb_4Se_8 layer [i.e., the (a + c)-direction for $K_2Sb_4Se_8$]. Thus, the thermal transport of $K_2Sb_4Se_8$ should occur largely along the b-direction, and that along the (a + c)-direction should be weak, and so should be that along the (a−c)-direction (i.e., the interlayer direction). We examine the phonon properties and the lattice thermal conductivity of $K_2Sb_4Se_8$ using the Phono3py[23] code combined with DFT calculations. The phonon dispersion relations calculated for $K_2Sb_4Se_8$ using the experimental structure, shown in Fig. 5a, reveal the presence of an imaginary vibrational frequency. This indicates that the crystal structure as determined by X-ray diffraction measurements has a structural

instability, suggesting the possibility that the real crystal structure has structural defects such as the charge density wave, local kinks, and fluctuations that are not detected by X-ray diffraction.[25] This imaginary frequency disappears when the phonon dispersion relations are calculated for the structure of $K_2Sb_4Se_8$ optimized by DFT calculations (Fig. 5b). Nevertheless, there exist low-frequency phonons, indicating the presence of a soft potential, which is associated most likely with the conformationally-flexible Sb–Se–Se–Sb bridges.

We calculate the lattice thermal conductivities by solving the linearized phonon Boltzmann equation with the single-mode relaxation time approximation, results of which are presented in Fig. 5c. As expected from the crystal structure of $K_2Sb_4Se_8$, the thermal conductivities decrease in the order, the Sb_4Se_6 chain direction > the interchain direction of the Sb_4Se_8 layer > the interlayer direction. The lattice thermal conductivity κ_{latt} of $K_2Sb_4Se_8$ is estimated to be 5.32 W mK^{-1}, which is comparable to that of PbTe (with calculated $\kappa_{latt} \approx 2$ W mK^{-1}),[26] a well-known material for low lattice conductivity. The low lattice thermal conductivity of $K_2Sb_4Se_8$ is attributed to a decreased mean free path resulting from the large unit cell parameters, the low dimensional structure, and the structural instability arising from the conformationally flexible Sb–Se(2)–Se(2)–Sb bridges. For each b–Se(2)–Se(2)–Sb bridge, the potential energy curve with respect to a small change in the ∠Sb–Se(2)–Se(2)–Sb dihedral angle should be soft. It is most likely that the soft motions of the crystal lattice involve the slipping of each Sb_4Se_6 chain against its neighboring Sb_4Se_6 chains within each Sb_4Se_8 layer. The Sb–Se(2)–Se(2)–Sb bridges would act as phonon
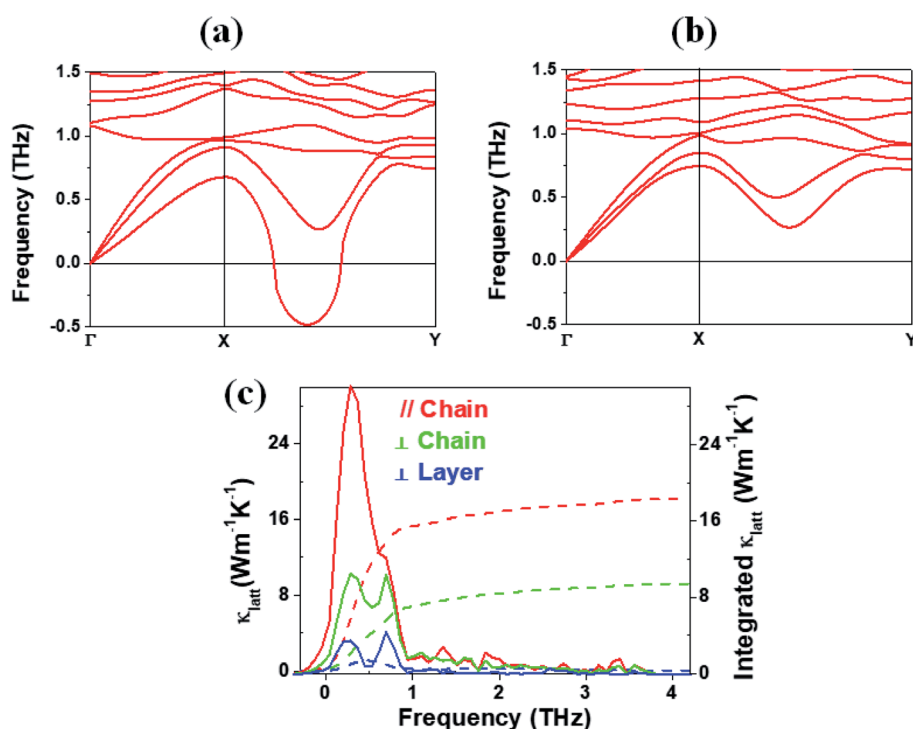

Fig. 5 Phonon dispersion relations calculated for (a) the experimental and (b) optimized structures of $K_2Sb_4Se_8$. (c) Lattice thermal conductivities κ_{latt} along the Sb_4Se_6 chain, along the interchain within the Sb_4Se_8 layer, and along the interlayer directions as a function of the frequency (solid lines). The integrated lattice thermal conductivities along the three directions are also shown (dashed lines).
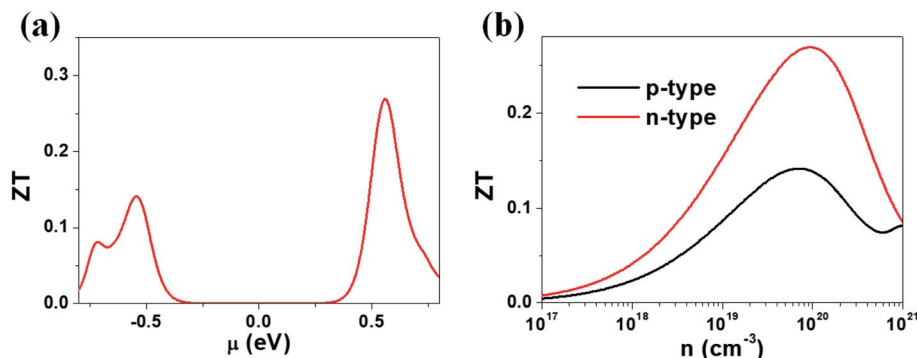
Fig. 6 ZT values calculated for $K_2Sb_4Se_8$ with $\tau \approx 2 \times 10^{-14}$ s: (a) the μ-dependence of the ZT using $\kappa_{latt} = 5.32$ W mK^{-1}. (b) The carrier density dependence of the ZT using $\kappa_{latt} = 5.32$ W mK^{-1}.

scattering centers rather than phonon transmittance paths due to their conformational flexibility. The lattice thermal conductivities of $Rb_2Sb_4Se_8$ and $Cs_2Sb_4Se_8$ should be similar to that of $K_2Sb_4Se_8$ because $Rb_2Sb_4Se_8$ and $Cs_2Sb_4Se_8$ are very similar to $K_2Sb_4Se_8$ in atomic and electronic structures.

Discussion

Our calculations suggest that the ternary selenides $A_2Sb_4Se_8$ (A = K, Rb, Cs) have high Seebeck coefficients, high power factors for the electron carriers, and low thermal conductivities. We estimate the ZT value of $K_2Sb_4Se_8$ at $T = 300$ K by using the calculated lattice thermal conductivity κ_{latt} of 5.32 W mK^{-1} and the relaxation time $\tau \approx 2 \times 10^{-14}$ s. In general, the relaxation time τ of conventional semiconductors is of the order of 10^{-14} s.[27] For example, the relaxation times $\tau \approx 2 \times 10^{-14}$ and 3×10^{-14} s reproduce the experimental resistivities of Bi_2Te_3 and PbTe, respectively.[27,28] The ZT values of $K_2Sb_4Se_8$ estimated by using $\tau \approx 2 \times 10^{-14}$ s are presented in Fig. 6. The μ-dependence of the ZT (Fig. 6a) shows a peak at $\mu \approx 0.56$ eV with $ZT \approx 0.27$, and another peak at $\mu \approx -0.54$ eV with $ZT \approx 0.14$. The dependence of ZT on the carrier densities (Fig. 6b) reveals a peak at the electron carrier density of $\sim 10^{20}$ cm^{-3}, which corresponds to the chemical potential $\mu \approx 0.56$ eV, and another peak at the hole carrier density of $\sim 7 \times 10^{19}$ cm^{-3}, which corresponds to the chemical potential $\mu \approx -0.54$ eV. The ZT of $K_2Sb_4Se_8$ is greater for the electron carriers than for the hole carriers by a factor of ~ 2. The calculated ZT values of $K_2Sb_4Se_8$ are comparable to those estimated for Bi_2Te_3.[27c,29]

We note that the electronic states crucial for determining the n-type (p-type) Seebeck coefficients are those lying mainly within ~ 0.5 eV from the CBM (VBM).[8] Such states of $A_2Sb_4Se_8$ (A = K, Rb, Cs) are represented largely by the Se(2) atoms forming the Sb–Se(2)–Se(2)–Sb bridges between two adjacent Sb_4Se_6 chains in each Sb_4Se_8 layer. Furthermore, the lattice thermal conductivity of $A_2Sb_4Se_8$ (A = K, Rb, Cs) is expected to be lowered by the Sb–Se(2)–Se(2)–Sb bridges because they are conformational flexible as mentioned above. Thus, in terms of both electronic and vibrational factors, the Sb–Se(2)–Se(2)–Sb bridges play a crucial role in enhancing the thermoelectric properties of $A_2Sb_4Se_8$ (A = K, Rb, Cs).

Concluding remarks

Our work suggests that the layered ternary selenides $A_2Sb_4Se_8$ (A = K, Rb, Cs) are a promising thermoelectric material comparable in efficiency to, or better than, the well-known thermoelectric materials such as Bi_2Te_3 and PbTe. The power factor and ZT values estimated for the electron carriers are considerably greater than those for the hole carriers by a factor of ~ 2. Thus, the ternary selenides $A_2Sb_4Se_8$ (A = K, Rb, Cs) are predicted to be a high-performance n-type thermoelectric material. The electronic and phonon structures associated with the Se(2)$_2$ dimer units of the conformationally-flexible Sb–Se(2)–Se(2)–Sb bridges are crucial in determining the thermoelectric properties of $A_2Sb_4Se_8$ (A = K, Rb, Cs).

Conflicts of interest

There are no conflicts to declare.

Acknowledgements

Notes and references

1 G. S. Nolas, J. Sharp and H. Goldsmid, *Thermoelectrics: Basic Principles and New Materials Developments*, Springer, New York, 2001.
2 D. M. Rowe, *Thermoelectrics Handbook: Macro to Nano*, CRC Press, Boca Raton, 2006.
3 A. J. Minnich, M. S. Dresselhaus, G. F. Ren and G. Chen, *Energy Environ. Sci.*, 2009, **2**, 466–479.
4 L. L. Baranowski, G. J. Snyder and E. S. Toberer, *J. Appl. Phys.*, 2013, **115**, 126102.
5 R. Franz and G. Wiedemann, *Ann. Phys.*, 1853, **165**, 497–531.

6 J. Q. He, M. G. Kanatzidis and V. P. Dravid, *Mater. Today*, 2013, **16**, 166–176.

7 L. D. Zhao, V. P. Dravid and M. G. Kanatzidis, *Energy Environ. Sci.*, 2014, **7**, 251–268.

8 (*a*) C. Lee, J. H. Shim and M.-H. Whangbo, *Inorg. Chem.*, 2018, **57**, 11895–11900; (*b*) C. Lee, J. N. Kim, J.-Y. Tak, H. K. Cho, J. H. Shim, Y. S. Lim and M.-H. Whangbo, *AIP Adv.*, 2018, **8**, 115213; (*c*) C. Lee, T.-H. An, E. E. Gordon, H. S. Ji, C. Park, J. H. Shim, Y. S. Lim and M.-H. Whangbo, *Chem. Mater.*, 2017, **29**, 2348–2354.

9 (*a*) S. Nakajima, *J. Phys. Chem. Solids*, 1963, **24**, 479–485; (*b*) N. Bouad, L. Chapon, R.-M. Marin-Ayral, F. Bouree-Vigneron and J. C. Tedenac, *J. Solid State Chem.*, 2003, **173**, 189–195.

10 W. S. Sheldrick and M. Wachhold, *Z. Kristallogr. NCS*, 1998, **213**, 25.

11 (*a*) W. S. Sheldrick and M. Wachhold, *Z. Kristallogr. NCS*, 1998, **213**, 24; (*b*) W. S. Sheldrick and J. Kaub, *Z. Anorg. Allg. Chem.*, 1986, **536**, 114–118.

12 J. R. Sootsman, D. Y. Chung and M. G. Kanatzidis, *Angew. Chem., Int. Ed.*, 2009, **48**, 8616–8639.

13 (*a*) P. E. Blöchl, *Phys. Rev. B: Condens. Matter Mater. Phys.*, 1994, **50**, 17953–17979; (*b*) G. Kresse and D. Joubert, *Phys. Rev. B: Condens. Matter Mater. Phys.*, 1999, **59**, 1758–1775.

14 G. Kresse and J. Furthmüller, *Phys. Rev. B: Condens. Matter Mater. Phys.*, 1996, **54**, 11169–11186.

15 J. P. Perdew, K. Burke and M. Ernzerhof, *Phys. Rev. Lett.*, 1996, **77**, 3865–3868.

16 G. K. H. Madsen and D. Singh, *Comput. Phys. Commun.*, 2006, **175**, 67–71.

17 G. K. H. Madsen, *J. Am. Chem. Soc.*, 2006, **128**, 12140–12146.

18 T. J. Scheidemante, C. Ambrosch-Draxl, T. Thonhauser, J. V. Badding and J. O. Sofo, *Phys. Rev. B: Condens. Matter Mater. Phys.*, 2003, **68**, 125210.

19 (*a*) L. Chaput, P. Pécheur, J. Tobola and H. Scherrer, *Phys. Rev. B: Condens. Matter Mater. Phys.*, 2005, **72**, 085126; (*b*) X. Gao, K. Uehara, D. D. Klug, S. Patchkovskii, J. S. Tse and T. M. Tritt, *Phys. Rev. B: Condens. Matter Mater. Phys.*, 2005, **72**, 125202.

20 D. J. Singh, *Phys. Rev. B: Condens. Matter Mater. Phys.*, 2010, **81**, 195217.

21 W. Chen, J.-H. Pöhls, G. Hautier, D. Broberg, S. Bajaj, U. Aydemir, G. M. Gibbs, H. Zhu, M. Asta, G. J. Snyder, B. Meredig, M. A. White, K. Perssonae and A. Jain, *J. Mater. Chem. C*, 2016, **4**, 4414–4426.

22 (*a*) C. Lee, J. Hong, M.-H. Whangbo and J. H. Shim, *Chem. Mater.*, 2013, **25**, 3745–3752; (*b*) C. Lee, J. Hong, W. R. Lee, D. Y. Kim and J. H. Shim, *J. Solid State Chem.*, 2014, **211**, 113–119.

23 A. Togo, L. Chaput and I. Tanaka, *Phys. Rev. B: Condens. Matter Mater. Phys.*, 2015, **91**, 094306.

24 (*a*) J. Hong, C. Lee, J.-S. Park and J. H. Shim, *Phys. Rev. B: Condens. Matter Mater. Phys.*, 2016, **93**, 035445; (*b*) J. Xin, Y. Tang, Y. Liu, X. Zhao, H. Pan and T. Zhu, *npj Quantum Mater.*, 2018, **3**, 9; (*c*) Y. Tang, Z. M. Gibbs, L. A. Agapito, G. Li, H.-S. Kim, M. B. Nardelli, S. Curtarolo and G. J. Snyder, *Nat. Mater.*, 2015, **14**, 1223–1228; (*d*) R. Hanus, X. Guo, Y. Tang, G. Li, G. J. Snyder and W. G. Zeier, *Chem. Mater.*, 2017, **29**, 1156–1164.

25 (*a*) H. B. Nielsen and M. Ninomiya, *Prog. Theor. Phys.*, 2005, **113**, 603–624; (*b*) H. Kim, C.-J. Kang, K. Kim, J. H. Shim and B. I. Min, *Phys. Rev. B: Condens. Matter Mater. Phys.*, 2015, **91**, 165130.

26 (*a*) Z. Tian, J. Garg, K. Esfarjani, T. Shiga, J. Shiomi and G. Chen, *Phys. Rev. B: Condens. Matter Mater. Phys.*, 2012, **85**, 184303; (*b*) J. M. Skelton, S. C. Parker, A. Togo, I. Tanaka and A. Walsh, *Phys. Rev. B: Condens. Matter Mater. Phys.*, 2014, **89**, 205203; (*c*) T. Shiga, J. Shiomi, J. Ma, O. Delaire, T. Radzynski, A. Lusakowski, K. Esfarjani and G. Chen, *Phys. Rev. B: Condens. Matter Mater. Phys.*, 2012, **85**, 155203.

27 (*a*) H.-W. Jeon, H.-P. Ha, D.-B. Hyun and J.-D. Shim, *J. Phys. Chem. Solids*, 1991, **52**, 579–585; (*b*) T. J. Scheidemantel, C. Ambrosch-Draxl, T. Thonhauser, J. V. Badding and J. O. Sofo, *Phys. Rev. B: Condens. Matter Mater. Phys.*, 2003, **68**, 125210; (*c*) B.-L. Huang and M. Kaviany, *Phys. Rev. B: Condens. Matter Mater. Phys.*, 2008, **77**, 125209.

28 S. Ahmad and S. D. Mahanti, *Phys. Rev. B: Condens. Matter Mater. Phys.*, 2010, **81**, 165203.

29 (*a*) I. T. Witting, T. C. Chasapis, F. Ricci, M. Peters, N. A. Heinz, G. Hautier and G. J. Snyder, *Adv. Electron. Mater.*, 2019, **5**, 1800904; (*b*) J. N. Kim, M. Kaviany and J.-H. Shim, *Phys. Rev. B*, 2016, **93**, 075119; (*c*) M.-Y. Han, Y. Jin, D.-H. Lee and S.-J. Kim, *Mater*, 2017, **10**, 1235.